

# Characterization of the $^{222}\text{Rn}$ family turbulent transport in the convective atmospheric boundary layer

J.-F. Vinuesa and S. Galmarini

European Commission - DG Joint Research Centre, Institute for Environment and Sustainability, Italy

Received: 2 June 2006 – Published in Atmos. Chem. Phys. Discuss.: 25 September 2006

Revised: 1 February 2007 – Accepted: 6 February 2007 – Published: 12 February 2007

**Abstract.** The combined effect of turbulent transport and radioactive decay on the distribution of  $^{222}\text{Rn}$  and its progeny in convective atmospheric boundary layers (CBL) is investigated. Large eddy simulation is used to simulate their dispersion in steady state CBL and in unsteady conditions represented by the growth of a CBL within a pre-existing reservoir layer.

The exact decomposition of the concentration and flux budget equations under steady state conditions allowed us to determine which processes are responsible for the vertical distribution of  $^{222}\text{Rn}$  and its progeny. Their mean concentrations are directly correlated with their half-life, e.g.  $^{222}\text{Rn}$  and  $^{210}\text{Pb}$  are the most abundant whereas  $^{218}\text{Po}$  show the lowest concentrations.  $^{222}\text{Rn}$  flux decreases linearly with height and its flux budget is similar to the one of inert emitted scalar, i.e., a balance between on the one hand the gradient and the buoyancy production terms, and on the other hand the pressure and dissipation at smaller scales which tends to destroy the fluxes. While  $^{222}\text{Rn}$  exhibits the typical bottom-up behavior, the maximum flux location of the daughters is moving upwards while their rank in the  $^{222}\text{Rn}$  progeny is increasing leading to a typical top-down behavior for  $^{210}\text{Pb}$ . We also found that the relevant radioactive decaying contributions of  $^{222}\text{Rn}$  short-lived daughters ( $^{218}\text{Po}$  and  $^{214}\text{Pb}$ ) act as flux sources leading to deviations from the linear flux shape. In addition, while analyzing the vertical distribution of the radioactive decay contributions to the concentrations, e.g. the decaying zone, we found a variation in height of  $^{222}\text{Rn}$  daughters' radioactive transformations.

Under unsteady conditions, the same behaviors reported under steady state conditions are found: deviation of the fluxes from the linear shape for  $^{218}\text{Po}$ , enhanced discrepancy in height of the radioactive transformation contributions for all the daughters. In addition,  $^{222}\text{Rn}$  and its progeny concen-

trations decrease due to the rapid growth of the CBL. The analysis emphasizes the crucial role of turbulent transport in the behavior of  $^{222}\text{Rn}$  morning concentrations, in particular the ventilation at the top of the boundary layer that leads to the dilution of  $^{222}\text{Rn}$  by mixing with radon low concentration air.

## 1 Introduction

$^{222}\text{Rn}$  is a naturally-occurring radioactive noble gas with a half-life of 3.8 days. Its unreactive nature makes it a suitable tracer in studies of atmospheric boundary layers (Pors-tendörfer, 1994). Ground-based measurements and vertical distributions of  $^{222}\text{Rn}$  and its daughters have been extensively studied in the past, e.g., to characterize the turbulent properties of the ABL, to perform regional and global circulation model benchmarking and to estimate regional surface fluxes of air pollutant and in particular climate-sensitive compounds. For a review on the use of  $^{222}\text{Rn}$  observations in atmospheric sciences see Zahorowski et al. (2004). Several authors (Larson et al., 1972; Lopez et al., 1974; Polian et al., 1986; Gaudry et al., 1990; Ramonet et al., 1996; Vinod Kumar et al., 1999) have shown that the study of the behavior of radon and its progeny is of great importance for air pollutant and greenhouse gases transport modeling. In particular,  $^{222}\text{Rn}$  is often used to calibrate and validate transport models (Genthon and Armengaud, 1995; Li and Chang, 1996; Jacob et al., 1997; Stockwell et al., 1998; Dentener et al., 1999).

The correlation between ground level radon concentrations and meteorological conditions in the lower atmosphere has been investigated in various occasions (e.g., Moses et al., 1963; Pearson and Moses, 1966; Ikebe, 1970; Druilhet and Fontan, 1973a and 1973b; Beck and Gogolak, 1979; Robé et al., 1992; Kataoka et al., 2001; Galmarini, 2006) including the relationship with the atmospheric stability (e.g., Wilkening, 1970; Guedalia et al., 1974; Fontan et al., 1979;

Correspondence to: J.-F. Vinuesa  
(jeff.vinuesa@jrc.it)

Guedalia et al., 1980; Fujinami and Esaka, 1987 and 1988; Kataoka et al., 1998; Sesana et al., 1998). It has also been used to investigate transport processes such as convection (Mahowald et al., 1997; Stockwell et al., 1998; Sesana et al., 2006), diurnal variability (Jacob and Prather, 1990; Kataoka et al., 1998), and synoptic variability of the ABL (Allen et al., 1996). However only few studies have addressed the vertical dispersion of radon and its daughters. For instance, Ikebe and Shimo (1972), Druilhet and Fontan (1973a, and 1973b) and Butterweck et al. (1994) estimated the vertical turbulent diffusivity from  $^{220}\text{Rn}$  measurement profiles, Jacobi and Andre (1963) and Beck and Gogolak (1979) evaluated the radon and its daughter products concentration profiles using a local gradient formulation for the fluxes assuming eddy diffusivities to be equal to eddy conductivity. Lopez et al. (1974) and Guedalia et al. (1973, and 1974) used aircraft data to extract information on the vertical transport while Vinod Kumar et al. (1999) used Wangara field experiment data set (Clarke et al., 1971) to analyze their model results.

Some of the radon radionuclides and their short-lived daughters have been used to study the turbulent diffusion process since they have half-lives of the same order of magnitude of the turnover time of the convective boundary layer (CBL). While the so-called long lived species are well mixed and the vertical flux profiles follow a linear shape (Wyngaard, 1985), the short-lived compound fluxes deviate from the inert linear profile. In this respect, accurate modeling requires a better understanding of how turbulence affects the dispersion of  $^{222}\text{Rn}$  and its progeny in atmospheric boundary layers. The scales associated with turbulent motions range from the Kolmogorov dissipation scale (on the order of a millimeter) to the boundary layer depth (on the order of a kilometer). The largest eddies are responsible for the turbulent transport of the scalars and momentum whereas the smallest ones are mainly dissipative. Thus, realistic numerical experiments of the atmospheric boundary layer require the use of large-eddy simulation (LES) that allows to explicitly solve relevant turbulent scales.

Previous LES studies have shown that the turbulent mixing can control the concentration and the distribution of reacting scalars in the CBL (Schumann, 1989; Sykes et al., 1994; Gao and Wesely, 1994; Verver et al., 1997; Molemaker and Vilà-Guerau de Arellano, 1998; Petersen et al., 1999; Petersen, 2000; Petersen and Holtslag, 1999; Krol et al., 2000; Patton et al., 2001; Vinuesa and Vilà-Guerau de Arellano, 2003; Vinuesa and Vilà-Guerau de Arellano, 2005). However, these studies have been mostly restricted to moderately fast reacting flows involving a second-order and/or a first order reaction. In particular, Vinuesa and Vilà-Guerau de Arellano (2003) performed a budget analysis of the fluxes and (co-)variances for second-order reacting scalars in a steady-state CBL. A key and novel aspect of this work is to extend the analysis to a chain of decaying species with a wide range of half-lives. Every new species decays with

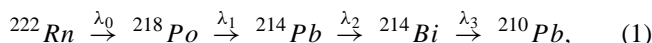
a timescale that varies from one to another. Its concentration will depend on its own decay but also on the decay of its mother. Thus the distribution of the new species will be affected by the mixing of the previous one in the chain.

To our knowledge, no study so far has analyzed the turbulent transport of  $^{222}\text{Rn}$  short-lived daughters in a CBL in a such comprehensive manner. We perform a complete analysis of the vertical distribution, reactivity and turbulent transport of  $^{222}\text{Rn}$  and its progeny under convective conditions. In order to account for all the relevant scales of the atmospheric boundary layer, we use LES to explicitly calculate the different terms of the concentration budget equations. The CBL analyzed here is considered under steady and unsteady conditions i.e. a fully developed CBL and a CBL growing within the reservoir layer resulting from the collapse of previous daytime CBL. In addition to the explicit calculation of the different contributions to concentration budget equations, the study under steady state conditions allows to perform a full budget analysis of the turbulent transport, i.e. the fluxes, and so to identify the driving process of  $^{222}\text{Rn}$  and its progeny concentration behavior. The analysis of the unsteady boundary layer aims at understanding the exchanges between the reservoir and the mixed layer while the boundary layer is deepening and so the turbulent timescale is increasing. In addition, the behavior of decaying species in this transient part of the day has never been studied before.

The structure of this paper is as follows. In Sect. 2, we present the chemical system of the  $^{222}\text{Rn}$  radioactive decaying chain together with the theoretical basis for concentration and flux budget decompositions. The numerical simulation specifications and the turbulent reacting flow classification are presented in Sect. 3. The vertical distribution, the reactivity and the transport by turbulence of  $^{222}\text{Rn}$  and its daughters in the case of the steady-state CBL are analyzed in Sect. 4. In Sect. 5, the results obtained under unsteady conditions are discussed. Finally, a summary is presented and conclusions are drawn in the last section.

## 2 $^{222}\text{Rn}$ decaying chain

We consider the radioactive decay chain of  $^{222}\text{Rn}$  that reads:



where  $\lambda_0$ ,  $\lambda_1$ ,  $\lambda_2$  and  $\lambda_3$  are the decay frequencies equal to  $2.11 \times 10^{-6}$ ,  $3.80 \times 10^{-3}$ ,  $4.31 \times 10^{-4}$ , and  $5.08 \times 10^{-4} \text{ s}^{-1}$ , respectively. Note that we consider a direct transformation of  $^{214}\text{Bi}$  into  $^{210}\text{Pb}$  since the half-life of  $^{214}\text{Po}$  (daughter of  $^{214}\text{Bi}$ ) is very short (164  $\mu\text{s}$ ). Also we consider  $^{210}\text{Pb}$ , that has a half-life of 22.3 years, as an inert scalar with respect to the temporal scales considered here. To increase readability,  $^{222}\text{Rn}$  and its progeny will also be referred to as  $S_i$  where  $i$  is the rank of the daughter in the decay chain from here on, e.g.  $S_0$  and  $S_4$  stand for  $^{222}\text{Rn}$  and  $^{210}\text{Pb}$ , respectively.

In the planetary boundary layer, under horizontally homogeneous conditions with no mean wind and neglecting the transport due to molecular diffusion, the temporal evolution of the mean concentrations  $S_i$  of a radionuclide reads

$$\frac{\partial S_i}{\partial t} = -\frac{\partial \overline{ws_i}}{\partial z} + R_{S_i} \quad (2)$$

where the horizontal averages are denoted both by capital letters and overbars whereas the fluctuations of the variables around the horizontal average value are represented by lower case letters. For the chain (1), the radioactive source/sink terms  $R_{S_i}$  are

$$R_{S_0} = -\lambda_0 S_0, \quad (3)$$

$$R_{S_1} = \lambda_0 S_0 - \lambda_1 S_1, \quad (4)$$

$$R_{S_2} = \lambda_1 S_1 - \lambda_2 S_2, \quad (5)$$

$$R_{S_3} = \lambda_2 S_2 - \lambda_3 S_3, \quad (6)$$

$$R_{S_4} = \lambda_3 S_3. \quad (7)$$

The vertical scalar flux budget equation reads

$$\begin{aligned} \frac{\partial \overline{ws_i}}{\partial t} = & \underbrace{-\overline{w^2} \frac{\partial S_i}{\partial z}}_G + \underbrace{\frac{g}{\Theta_0} \overline{\theta s_i}}_B - \underbrace{\frac{\partial \overline{w^2 s_i}}{\partial z}}_T - \underbrace{\overline{s_i} \frac{\partial \pi}{\partial z}}_P \\ & - \underbrace{\overline{s_i} \frac{\partial \tau_{3j}}{\partial x_j} - \overline{w} \frac{\partial \langle u''_j s''_i \rangle}{\partial x_j}}_D + \underbrace{R_{\overline{ws_i}}}_{CH}, \end{aligned} \quad (8)$$

where  $w$ ,  $\theta$  and  $s_i$  represent the fluctuation of the vertical velocity, the temperature and the reactant concentration, respectively.  $\Theta_0$  is a reference state potential temperature,  $S_i$  is the horizontal average reactant quantity and  $\pi$  is the modified pressure defined as  $[(p - p_0)/\rho_0] + (2/3)E$ , where  $p$ ,  $p_0$  and  $\rho_0$  are the pressure, a reference pressure and a reference density respectively, and  $E$  is the subgrid-scale turbulent kinetic energy. The subgrid stress for momentum and scalar are represented by  $\tau_{3j}$  and  $\langle u''_j s''_i \rangle$  respectively. The terms on the right-hand side are the mean gradient term (G), the buoyancy (B), the turbulent transport (T), the pressure term (P), the dissipation (D) and the chemical or radioactive decay contribution (CH). The description of the flux temporal evolution is of importance to identify the driven processes involved in the turbulent dispersion of  $^{222}\text{Rn}$  and its progeny.

The radioactive decay terms in the budget equations are

$$R_{\overline{ws_0}} = -\lambda_0 \overline{ws_0}, \quad (9)$$

$$R_{\overline{ws_1}} = \lambda_0 \overline{ws_0} - \lambda_1 \overline{ws_1}, \quad (10)$$

$$R_{\overline{ws_2}} = \lambda_1 \overline{ws_1} - \lambda_2 \overline{ws_2}, \quad (11)$$

$$R_{\overline{ws_3}} = \lambda_2 \overline{ws_2} - \lambda_3 \overline{ws_3}, \quad (12)$$

$$R_{\overline{ws_4}} = \lambda_3 \overline{ws_3}. \quad (13)$$

**Table 1.** Initial values and prescribed surface fluxes used for both simulations.

	Steady-state CBL	Unsteady CBL
	(1)	(2)
$z_i$	662.5 m	187.5 m
$\Theta_m$	288 K	286 K
$\Delta\Theta$	5 K	
$\overline{(w\theta)}_s$	0.052 K m s <sup>-1</sup>	
$\gamma_\theta$	$6 \times 10^{-3}$ K m <sup>-1</sup>	

### 3 Description of the numerical simulations

The capacity of LES to simulate extremely accurately turbulent condition of atmospheric boundary layers has been widely proved over the years through extensive comparison with laboratory and field measurements. We use the three-dimensional LES code described by Cuijpers and Duynkerke (1993), Siebesma and Cuijpers (1995), Cuijpers and Holtslag (1998) and Vilà-Guerau de Arellano and Cuijpers (2000).

#### 3.1 Specifications of the simulated boundary layers

Two representative cases are investigated: a fully developed free convective atmospheric boundary layer and a CBL growing overlaid by a reservoir layer resulting from the collapse of the previous daytime CBL. For both cases, the modeling domains represent  $6.4 \text{ km} \times 6.4 \text{ km} \times 1.5 \text{ km}$  with a vertical and horizontal resolutions of 25 and 50 m respectively, leading to  $128 \times 128 \times 60$  grid-points simulations. Periodic lateral boundary conditions are assumed. The maximum time-step used in the calculations is 0.5 s.

As radon and its daughters are unaffected by moisture, the simulated atmospheric boundary layers (ABL) are dry, convective ABLs driven by buoyancy only (see Table 1 and Fig. 1).

In the steady-state CBL,  $^{222}\text{Rn}$  is emitted at the surface with a flux of  $0.5 \text{ Bqm}^{-2} \text{ s}^{-1}$ . All radionuclides have a zero initial profile except  $^{222}\text{Rn}$ . The latter is the result of a pre-run of 1 hour simulation with the same surface flux, no initial concentration and a decay constant set to zero. The simulation is running for 8 h with a pre-run of 1 h for the dynamics. The statistics and the budget analysis are done on the last hour of the simulation. The convective velocity scale  $w_*$ , the ABL height  $z_i$  (defined as the depth where the sensible heat flux is minimum) and the free convection time-scale  $t_* \equiv z_i/w_*$  are equal to  $1.12 \text{ ms}^{-1}$ , 800 m and 714.3 s, respectively.

For the unsteady convective BL, we follow a special procedure to initialize  $^{222}\text{Rn}$  and its daughters profiles in order to ensure consistency regarding the assumption of radioactive

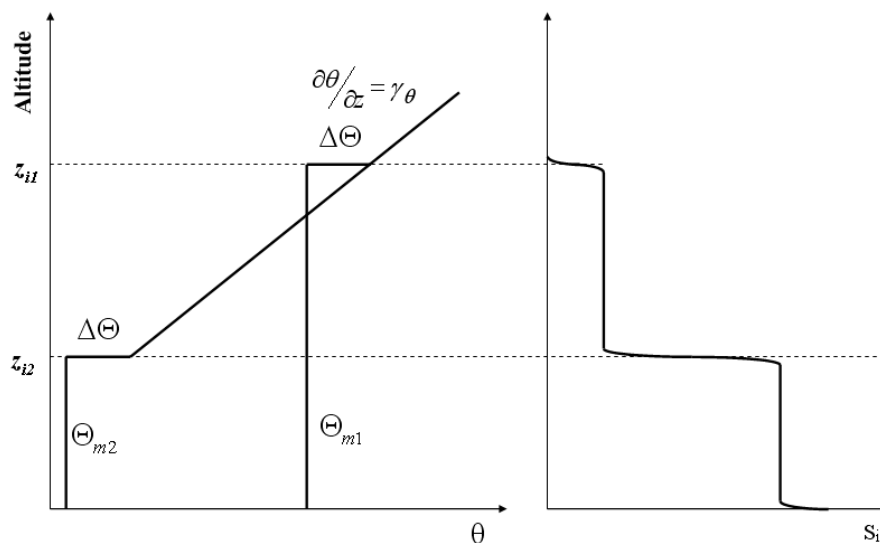


**Fig. 1.** Schematic representation of the experimental set-ups for the mean potential temperature  $\Theta_m$  (1- steady state and 2- unsteady simulations) and the mean  $S_i$  concentration in the unsteady CBL simulation (see the text for a definition of the different quantities shown above).

equilibrium of  $^{222}\text{Rn}$  and its progeny. Briefly, the resulting steady-state CBL of the previous simulation is divided into two regions: a nocturnal boundary layer of depth  $z_{i2}$  and a reservoir layer. Since the reservoir layer is assumed decoupled from the surface, no fresh radon is transported to this region during the 8-h' night. In the nocturnal boundary layer, a  $^{222}\text{Rn}$  surface flux of  $0.5 \text{ Bqm}^{-2} \text{ s}^{-1}$  is assumed constant during the night. In both regions, the  $^{222}\text{Rn}$  and its daughters profile concentrations are analytically calculated as the result of a 8 h period of radioactive activity from the resulting profiles of the previously simulated steady-state CBL (see the appendix). The simulation of the unsteady CBL is starting at sunrise and is running for 8 h.

Similar convective boundary layers and turbulent atmospheric reacting flows have been successfully simulated using the same SGS models that we used and even coarser resolutions. In particular, Jonker et al. (2004) used  $128 \times 128 \times 50$  grid-points for a domain of  $12.8 \text{ km} \times 12.8 \text{ km} \times 1.25 \text{ km}$  to simulate (among others) first order decaying scalars with turbulent Damköhler numbers up to 10. In our simulations, the biggest turbulent Damkhler number is found for  $S_1$  and is equal to 2.71 (see Table 2). In addition, we also performed simulations with coarser resolution ( $64 \times 64 \times 60$  grid-points) that didn't reveal any resolution dependency of the results. Thus, the results presented in the paper are not dependent on the choice of the SGS model.

In order to investigate the possible dependency of our results to the strength of the potential temperature inversion at the top of the CBL or to the forcing imposed by the surface heat flux, several additional simulations were performed. We simulated 3 extra steady-state cases with weaker inversion

strengths. We used initial potential temperature jumps at the top of the CBL of 1, 2 and 3 K. We also performed extra simulations of the unsteady case based on weaker inversion strengths and stronger surface heat fluxes. We used initial potential temperature jumps of 3, 3 and 5 K combined with surface heat fluxes of  $0.052$ ,  $0.1$  and  $0.1 \text{ K m s}^{-1}$ , respectively. In addition, unsteady simulation with the surface diurnal variation of the surface heat flux (from  $0.05$  to  $0.2 \text{ K m s}^{-1}$ ) and an initial potential temperature jump of 2.5 K. Using the usual boundary layer scaling parameters such as the CBL depth or the convection velocity scale yield to inversion strengths independent results in the steady state boundary layer. In the case of the unsteady growth of the boundary layer, we found similar results except that different forcing at the surface and capping at the top affect the boundary layer growth. However, the same discussion can be done and the same conclusions can be drawn as the ones presented in the following.

### 3.2 Reacting turbulent flow classification

The relative influence of turbulence on the species transformations can be quantified by the so-called turbulent Damköhler number  $Da_t$  (Damköhler, 1940), defined as the ratio between the integral time-scale of turbulent ( $\tau_t$ ) and the chemical time-scale ( $\tau_c$ ) that is, in this context, the decay time-scale of the radionuclide. Using this number, turbulent reacting flows can be classified into three categories (Schumann, 1989; Molemaker and Vilà-Guerau de Arellano, 1998; Krol et al., 2000; Vilà-Guerau de Arellano, 2003). For reacting flows with  $Da_t < 1$ , the transformation proceeds at a slower rate than the turbulent mixing. Therefore, mixing

**Table 2.** Volume averages of the turbulent Damköhler numbers.

Radionuclide	Steady-state CBL	Unsteady CBL
$S_0$	<0.01	<0.01
$S_1$	2.71	1.21–2.24
$S_2$	0.31	0.14–0.25
$S_3$	0.36	0.16–0.30

is reached prior to the transformations. When  $Da_t \approx O(1)$ , i.e. the time-scale of the transformation is of similar order to the time-scale of the turbulent mixing, atmospheric turbulence controls the transformations. The behavior of active species can differ from the behavior observed and modeled of inert scalars. In the case of a decaying scalar, the effect of turbulent mixing will affect the spatial distribution of the radionuclides. For  $Da_t \gg 1$ , transformations are much faster than the turbulent mixing meaning that species are transformed in-situ and are almost not transported. In our simulations,  $\tau_t = z_i/w_*$  and  $\tau_c = \lambda_j^{-1}$  with  $j=0, 1, 2, 3$ . The corresponding  $Da_t$  are summarized in Table 2. These numbers indicate that  $^{218}\text{Po}$  ( $S_1$ ) is strongly influenced by the turbulent mixing of the CBL in both steady and unsteady conditions. The other short-lived daughters  $^{214}\text{Pb}$  ( $S_2$ ) and  $^{214}\text{Bi}$  ( $S_3$ ) refer to a moderate-slow regime indicating that their distributions are only slightly affected by the combined effects of decay and mixing.

While studying the relevance of accounting for the chemical contribution to second-order moments (fluxes and (co-)variances) of reacting scalars, Vinuesa and Vilà-Guerau de Arellano (2003) extended the turbulent reacting flow classification by deriving other dimensionless numbers, the so-called Damköhler numbers for fluxes and (co-)variances. These numbers use a chemical time-scale based on the chemical terms included in second-order moment budget equations. They showed that for flux and (co-)variance Damköhler numbers  $\sim O(1)$ , the contribution of chemical terms to second-order moment profiles is significant. The flux Damköhler number can be expressed as the ratio of the flow time-scale to the time-scale of the chemical contribution to the flux. For a scalar  $B$  involved the chain



the flux Damköhler number reads

$$Da_{\overline{wb}} = \left| Da_{t,B} - Da_{t,A} \frac{w_* s_{A*}}{w_* s_{B*}} \right|. \quad (15)$$

By using the  $w_* s_{i*}$  proposed by Cuijpers and Holt-slag (1998), i.e.  $w_* s_{i*} = \frac{1}{z_i} \int_0^{z_i} \overline{ws_i} dz$ , and chemical time-scales based on the radioactive decaying terms included in flux budget equations, we calculate the flux Damköhler numbers and report them in Table 3. In the steady state CBL, significant effects of the radioactive decay contribution on the

**Table 3.** Volume averages of the flux turbulent Damköhler numbers.

Radionuclide	Steady-state CBL	Unsteady CBL
$S_0$	<0.01	<0.01
$S_1$	1.08	0.62–0.38
$S_2$	0.85	0.06–0.09
$S_3$	0.16	0.01–0.02
$S_4$	<0.01	<0.01

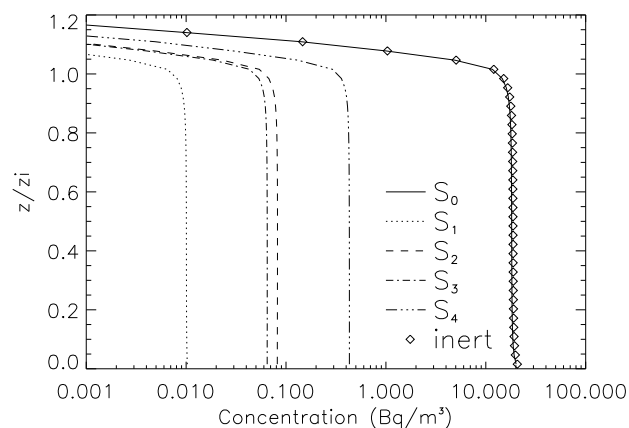


**Fig. 2.** Vertical profiles of  $^{222}\text{Rn}$  and its progeny concentrations. The legend numbers represent the rank of the decaying compound in the radioactive decay chain. The diamonds account for the concentration of an inert scalar emitted at the surface with the same flux as  $^{222}\text{Rn}$ .

flux for  $^{218}\text{Po}$  ( $S_1$ ) and  $^{214}\text{Pb}$  ( $S_2$ ) can be expected whereas  $^{214}\text{Bi}$  ( $S_3$ ) flux Damköhler number only indicates a small contribution of the decaying process. However, under unsteady conditions only  $^{218}\text{Po}$  ( $S_1$ ) flux is affected by the control exerts by turbulence on the radioactive decay contribution.

## 4 Dispersion of $^{222}\text{Rn}$ and its progeny in the steady-state CBL

### 4.1 Vertical distribution and radioactive decay contribution

Figure 2 shows the vertical profile of  $^{222}\text{Rn}$  and its progeny concentrations. The mixed-layer concentrations are correlated with the half-lives of the radionuclides; the faster decaying the daughter is, the smaller is the concentration. Also as indicated by the Damköhler number classification,  $^{222}\text{Rn}$  concentration only shows a small deviation from the inert scalar one. All the radionuclides show overall well-mixed profiles however since a wide range of radioactive decay frequencies is considered, e.g. from some minutes to days, any

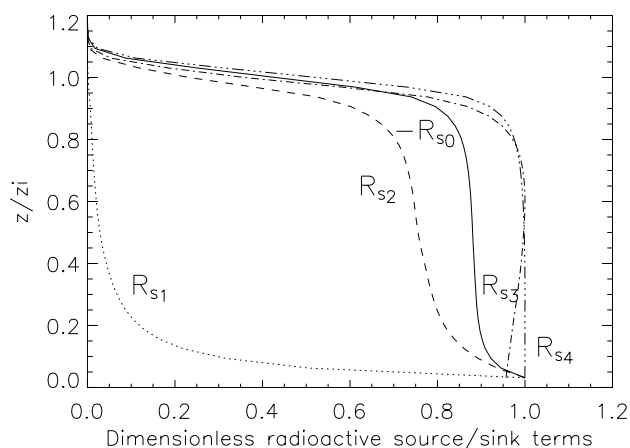


**Fig. 3.** Vertical profiles of the radioactive decay contribution to the concentration budget equations. The profiles are made dimensionless by using their maximum value. Note that the minus decay term of the  $^{222}\text{Rn}$  concentration budget is plotted to increase readability.

vertical variation can have an important impact on the radioactive transformations.

We explicitly calculate the radioactive decay contributions to the concentration budget equations and we show the resulting profiles in Fig. 3. As can be expected for  $S_0$  and since its radioactive decay contribution is proportional to its concentration, the radioactive decay is acting as a sink with a constant value within the mixed layer. For radon's daughters, the radioactive decay terms are composed of a balance between production by the decay of their mother and destruction but their own decay. For all the daughters, the radioactive decay contributions show an imbalance in favor of their production. Thus, as long as  $S_0$  is injected in the steady-state CBL, their concentration will grow with time and this is the direct evidence of the competition between mixing and decaying process. However, one can notice that the daughters' radioactive decay contribution are quite different in the vertical and that, apart  $R_{S_4}$  and to some extent  $R_{S_0}$ , none of them shows a constant value in the mixed layer.

Since  $S_1$  is the first daughter of the family, its production by the decay of  $S_0$  is more important where the  $^{222}\text{Rn}$  concentrations are higher, i.e. close to the surface. The radioactive decay of  $S_1$  proceeds at a faster rate than the turbulent mixing meaning that freshly created  $S_1$  are decaying before being well mixed in the CBL. As a result, the shape of the profile is quite different from the  $S_0$  one showing a fast reduction while moving upward. For the daughters with a longer half-life than  $S_1$ , turbulence is more efficient to mix freshly created daughters with older ones but still some vertical variation can be noted for  $S_2$  and  $S_3$ . For the latter, one can notice a very interesting behavior: while all other radioactive contributions are more important close to the surface, the one of  $S_3$  shows a maximum contribution at around  $0.6 z/z_i$ . The decaying term  $R_{S_3}$  in the  $S_3$  concentration budget equation

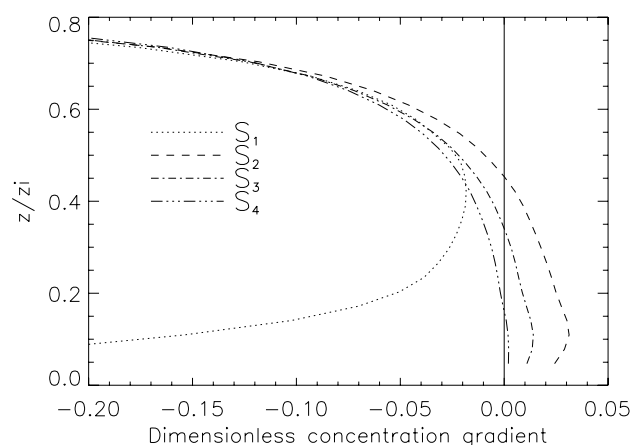


**Fig. 4.** Vertical profiles of the dimensionless concentration gradient of  $^{222}\text{Rn}$  short-lived daughters  $S_1$ ,  $S_2$ ,  $S_3$  and  $S_4$ . The profiles are scaled with the daughters' maximum CBL concentration and made dimensionless by  $z_i$ . To increase readability, only the part of the CBL where discrepant profiles are found is shown.

is composed of a source term and a sink term. The source term is the production by radioactive decay of  $S_2$ , i.e.  $\lambda_2 S_2$ , and the sink term is its own radioactive decay, i.e.  $\lambda_3 S_3$ . This latter sink term is equal to the radioactive decay contribution  $R_{S_4}$ . Since  $S_4$  radioactive decay contribution shows a constant profile at lower altitudes, one can assume that  $S_3$  is well-mixed at these depths. However from the surface to  $0.6 z/z_i$ ,  $R_{S_3}$  increases suggesting an imbalance between its own radioactive decay and the production by the decay of  $S_2$ . Since the radioactive decay of  $S_2$  is proportional to  $S_2$  concentration, we can conclude that  $S_2$  is inefficiently mixed by turbulence and that it has higher CBL concentration at the mid-CBL than at the surface.

As noticed previously, the concentration profiles shown in Fig. 2 look overall well-mixed which can be found discrepant with the inhomogeneous  $R_{S_i}$  vertical profiles. However, a closer look to the concentrations or to the concentration gradients for instance (Fig. 4) reveals inhomogeneous mixing of the daughters. While  $S_1$  and  $S_4$  decrease with height,  $S_2$  and  $S_3$  have positive gradients up to the mid-CBL that is in agreement with the analysis of the  $R_{S_i}$ .  $S_1$  production is higher close to the emission source of  $S_0$  and since  $S_1$  is transformed at a faster rate than it is transported (with  $Da_t=2.71$ ), freshly created  $S_1$  are decomposed into  $S_2$  preferentially at around mid-CBL. This clearly shows the relevance of accounting for the influence of turbulent mixing on the dispersion of  $^{222}\text{Rn}$  short-lived daughters.

## 4.2 Turbulent transport

Within the boundary layer, the profiles of inert scalars have a linear shape (Deardorff, 1979; Wyngaard and Brost, 1984; Wyngaard, 1985) whereas the fluxes of reacting scalars

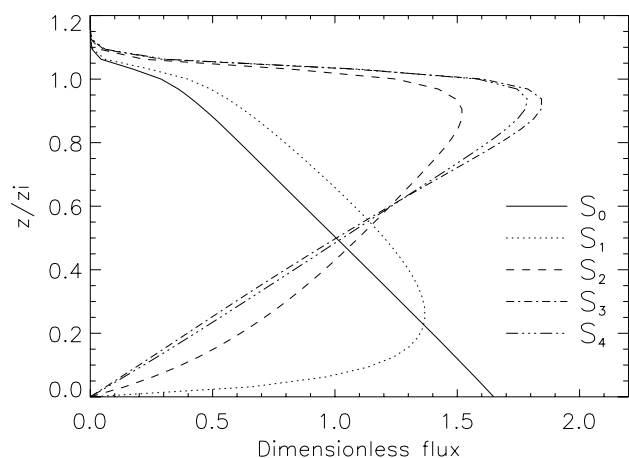


**Fig. 5.** Vertical profiles of the dimensionless fluxes for  $^{222}\text{Rn}$  and its daughters. The values are made dimensionless by  $w_*s_{i*}$  as proposed by Cuijpers and Holtslag (1998).

show deviations with from this shape correlated with their Damköhler numbers (Gao and Wesely, 1994; Sykes et al., 1994; Vinuesa and Vilà-Guerau de Arellano, 2003). These deviations are due to the action of the chemistry that can act as a sink or a source term in the flux budget.

The fluxes of  $S_0$  and its progeny are shown in Fig. 5. The fluxes of  $S_0$  and  $S_4$  have a linear profile whereas the ones of the other daughters show deviations from the linear shape. The flux of  $^{222}\text{Rn}$  is similar to an inert scalar flux. Thus the chemical term, that is the radioactive decay in our case, has no impact on the vertical transport of  $^{222}\text{Rn}$  as its Damköhler and flux Damköhler numbers suggested with  $Da_t < 0.01$  and  $Da_{ws_0} < 0.01$ .  $S_1$  has the highest Damköhler number ( $Da_t = 2.71$ ) and its flux shows the biggest deviation. The other short-lived daughters, i.e.  $S_2$  and  $S_3$ , have similar  $Da_t$  but while the deviation of  $S_2$  flux is significant, the one of  $S_3$  is rather small. Using the appropriate Damköhler number to assess the relevance of radioactive decay contribution to the flux allows clarifying this discrepancy. The flux Damköhler number for  $S_2$  is 0.85 while the one of  $S_3$  equals 0.16 suggesting the vertical transport of  $S_2$  is the one most significantly affected by turbulence.

The most interesting point is that the vertical distribution of the fluxes changes from one daughter to another. For  $S_0$ , the maximum flux is found at the surface where it is emitted. Since all daughters are produced by the radioactive decomposition of  $S_0$ , one would expect to find maximum daughter fluxes close to the surface. However and as can be clearly noticed in Fig. 5, this is not the case and the maximum flux location is moving upwards while the rank of the daughter in the  $^{222}\text{Rn}$  progeny is increasing.  $S_1$  has its maximum flux at  $0.25 z/z_i$  and the others daughters maximum fluxes are located around  $0.9 z/z_i$ . Actually, the maximum flux location reaches a quasi steady state value between  $0.90$  and  $0.95 z/z_i$

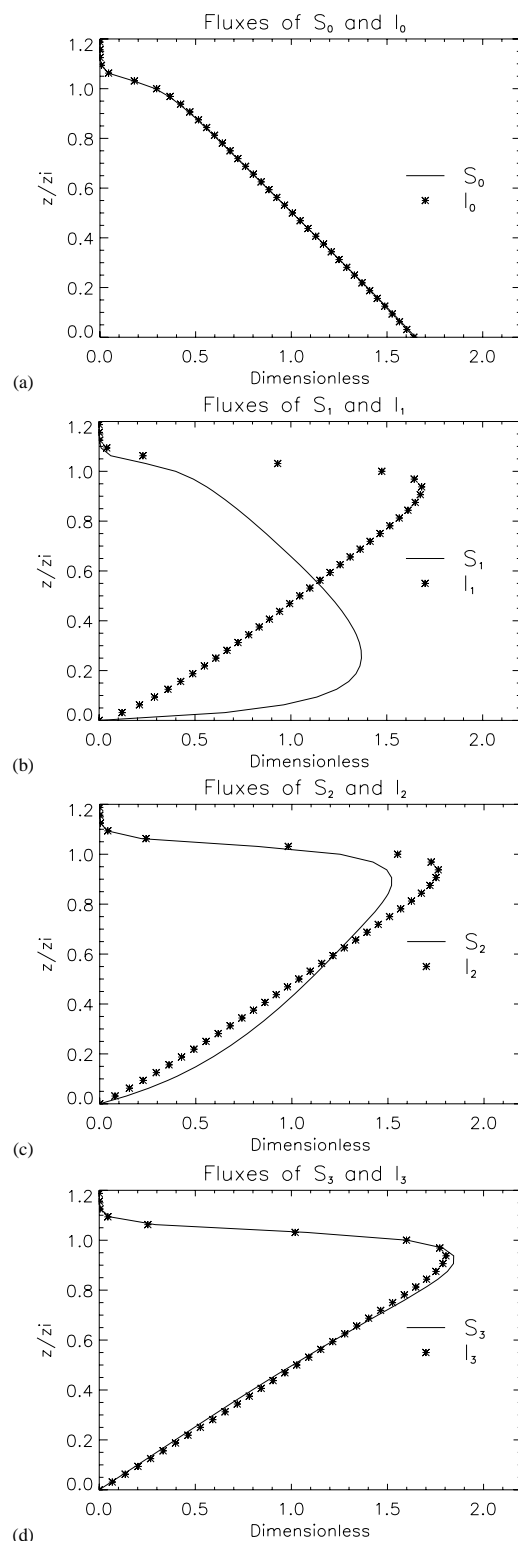


**Fig. 6.** Vertical profiles of the dimensionless fluxes for  $^{222}\text{Rn}$ , its daughters and the inert tracers. The values are made dimensionless by  $w_*s_{i*}$  as proposed by Cuijpers and Holtslag (1998).

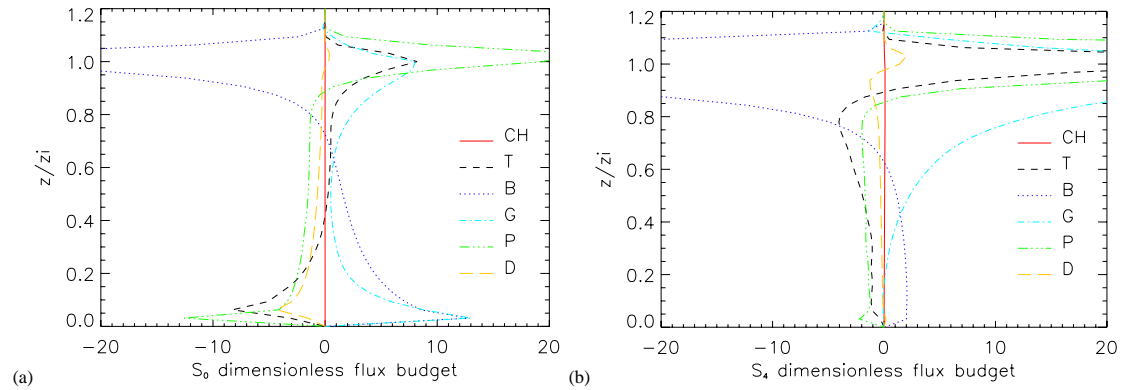


**Fig. 7.** Vertical profiles of the different contributions flux budget equations of (a)  $^{222}\text{Rn}$  ( $S_0$ ) and (b)  $^{210}\text{Pb}$  ( $S_4$ ). The profiles are made dimensionless using  $w_*^2 s_i z_i^{-1}$ .

for the slowest (in the flux Damköhler number sense) daughters, i.e.,  $S_3$  and  $S_4$ .

In order to show the relevance of the turbulent flux Damköhler number, one has to compare the evolution of the radionuclides to that of inert tracers released in the atmosphere at the same rate, location and time as the radionuclides. Thus, we design a hypothetical decaying chain involving inert scalars that are produced as the  $^{222}\text{Rn}$  progeny. For this academic case, we assume that each radionuclide produces a radioactive daughter and an inert daughter. This decaying pathway reads:

$$S_0 \xrightarrow{\lambda_0} S_1 + I_1, \quad (16)$$

$$S_1 \xrightarrow{\lambda_1} S_2 + I_2, \quad (17)$$

$$S_2 \xrightarrow{\lambda_2} S_3 + I_3, \quad (18)$$

where  $I_i$  is the inert daughter created by the mother  $S_{i-1}$ . Fig. 6 shows a comparison of the  $S_i$  and  $I_i$  fluxes.  $S_1$  has the biggest flux Damköhler number ( $Da_{wS_1}=1.08$ ) and its flux shows the most important deviation for the inert flux shape while the flux of  $S_3$  ( $Da_{wS_3}=0.16$ ) is only slightly different from  $I_3$  flux. This comparison clearly shows a correlation between the flux Damköhler number and the deviation of the radionuclide fluxes from the inert scalar shapes.

The understanding of the changes of flux profile shape behaviors through  $^{222}\text{Rn}$  progeny requires the determination of which physical processes are responsible for their fluxes. Therefore, in order to study the relevance of the radioactive decay contribution to the flux, the terms of the flux budget Eq. (8) have been calculated explicitly. For an inert emitted scalar, our results are similar to previous studies (Deardorff, 1974; Moeng and Wyngaard, 1984) and will not be presented here. Briefly, the budget for inert emitted scalar reveals a balance between the gradient and the buoyancy production terms on the one hand, which are the major flux sources up to the middle of the boundary layer, and on

the other hand the pressure and dissipation at smaller scales which tend to destroy the fluxes. The transport contribution is removing flux from the lower boundary layer upwards with a maximum dissipating effect close to the surface.

Figure 7 shows the vertical profiles of the different contribution to the fluxes of  $S_0$  and  $S_4$ . Both have a negligible radioactive decay contribution.  $S_0$  flux shows the typical decomposition obtained for bottom-up inert scalar (with a maximum flux at the surface) and  $S_4$  flux shows the one of a top-down inert scalar (with a maximum flux at the top of the CBL). For this latter, we found similar results to the work of Cuijpers and Holtslag (1998) and in particular their case *a1*. The gradient contribution becomes very small in the lower boundary layer where the main production due to buoyancy is balanced by the pressure correlation and the turbulent transport contributions. Turbulent transport is transporting flux upward with its maximum dissipative contribution is located around  $0.8 z/z_i$ . For  $S_0$  and  $S_4$ , accounting for the radioactive decay contribution to the flux is not relevant as was suggested by their very low flux Damköhler numbers (Table 3).

In Fig. 8, the vertical contributions to the flux budget equations of the other daughters are presented. We found that the radioactive decay term is responsible for a relevant part of the flux production for  $S_1$  and  $S_2$  whereas it is almost negligible for  $S_3$ . This is again in agreement with the flux Damköhler numbers presented in Table 3. The gradient production, i.e.,  $w^2 \frac{\partial S_i}{\partial z}$ , is the most affected term meaning that the radioactive decay is responsible for the decrease of the concentration gradient. The gradient term is reduced to one half of the  $S_0$  value and equals the radioactive decay contribution in the lower boundary layer in the case of  $S_1$ . In the  $S_2$  flux budget, it is actually dissipating flux in the same region. Its contribution becomes small but remains negative for  $S_3$  and it reaches a zero contribution for  $S_4$  (see Fig. 7 of this paper and Fig. 3c of Cuijpers and Holtslag (1998) to compare to a top-down inert scalar). The other term that is showing differences while



comparing flux budget contribution from the daughters is the turbulent transport contribution, i.e.,  $\frac{\partial w^2 s_i}{\partial z}$ . In the case of  $S_1$  the turbulent transport is extracting more flux from the lowest levels while for  $S_2$  and  $S_3$  the transport has an almost constant dissipating contribution for all levels below  $0.8 z/z_i$ . The results shown in Figs. 7 and 8 suggest that the radioactive decay is primarily acting on the concentration gradients leading to an important reduction of the gradient contribution to the flux and even a change of the contribution, i.e. to production from dissipation, especially for  $S_2$ . To a less important extent, the turbulent transport is also affected showing an enhancement of the transfer of flux from the lower levels to the top of the CBL.

These findings combined with the analysis of the radioactive contributions to the evolution of the mean concentrations presented in Fig. 3 lead to the conclusion that atmospheric turbulence controls the distribution of  $S_1$ ,  $S_2$  and  $S_3$ .

## 5 Dispersion of $^{222}\text{Rn}$ and its progeny under unsteady conditions

In this section, we extend our analysis to atmospheric boundary layers under unsteady conditions focusing on a CBL growing within an overlaid reservoir layer. Our study aims at understanding the exchanges between the reservoir and the mixed layer while the boundary layer is deepening (from 187.5 m to 600 m) and so the turbulent timescale is increasing (from 306.5 s to 605.9 s). In addition, the behavior of decaying or reacting species in this transient part of the day has never been fully studied before.

### 5.1 Vertical distribution

In Fig. 9, we show the time evolution of the concentration of the mother  $^{222}\text{Rn}$  ( $S_0$ ) and the last daughter of the chain  $^{210}\text{Pb}$  ( $S_4$ ). The other daughters are not shown since they have the same overall behavior as  $S_0$ . No fresh emissions of  $S_0$  reach the reservoir layer since it is almost decoupled from the surface. As a result,  $S_0$  (and the other daughters except  $S_4$ ) concentration decreases with time. Since  $S_4$  is the last daughter of the chain and is considered as an inert scalar, its concentration increases with time following the chain decaying process.

As the boundary layer deepens with time, the  $S_0$  mixed-layer concentration collapses despite of fresh emission. This collapse is due to both the dilution of  $S_0$  in an increasing volume and the entrainment of  $S_0$  low concentration air from the reservoir layer. The same behavior is observed for the other daughters (except  $S_4$  that shows CBL concentrations enhancing with time). Their concentrations are the result of antagonist effects: the production by the decaying chain, the dilution by boundary layer deepening and the ventilation due to the entrainment of lower concentration air masses from the reservoir layer. The production by the radioactive de-

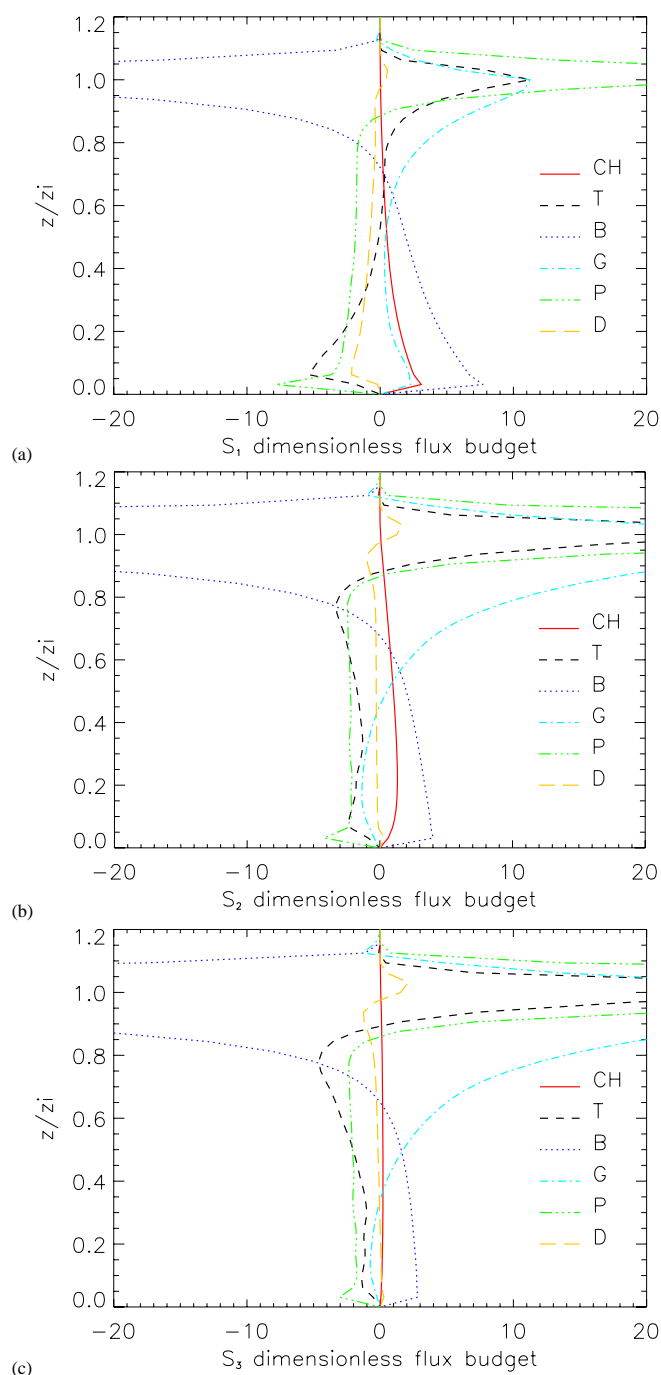


**Fig. 8.** Vertical profiles of the contributions to the flux budget equations of (a)  $^{218}\text{Po}$  ( $S_1$ ), (b)  $^{214}\text{Pb}$  ( $S_2$ ) and (c)  $^{214}\text{Bi}$  ( $S_3$ ). The profiles are made dimensionless using  $w_*^2 s_i z_i^{-1}$ .

causing contribution is not sufficient to balance the dilution and the ventilation leading to a decrease of the mixed-layer concentrations. However, in the case of  $S_4$ , one can notice that its concentration increases in the reservoir layer since it is considered as an inert and thus as the last product of the decaying chain. This increase limits the ventilation effect due

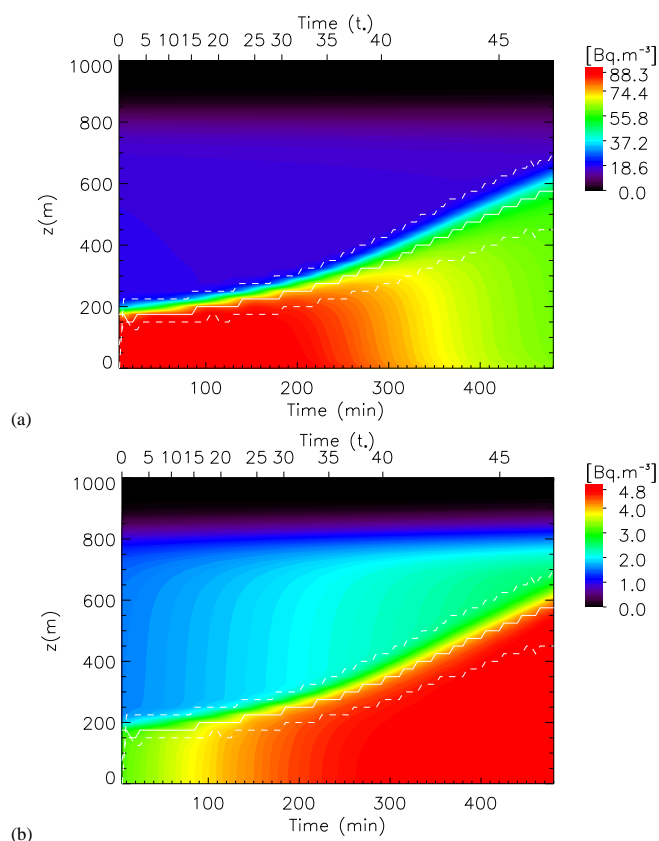


**Fig. 9.** Vertical profiles of (a)  $^{222}\text{Rn}$  ( $S_0$ ) and (b)  $^{210}\text{Pb}$  ( $S_4$ ) concentrations. The top of the CBL is overlotted with a white solid line and the entrainment layer is located between the dashed white lines. The steppy aspect of these latter quantities is due to averaging procedures, e.g. the CBL depth and the entrainment layer locations are determined from the 5 min slab averaged sensible heat flux. The concentrations are plotted against time in minutes (lower x-axis) and in  $t_*$  (upper x-axis) where  $t_* = z_i/w_*$ .

to vertical transport at the entrainment layer. In this case, the combined effect of dilution and detrainment do not balance the production by the radioactive decay and, as a result,  $S_4$  concentration increases with time in the CBL.

## 5.2 Radioactive decay and turbulent transport contributions

The time evolution of the concentrations is the result of the combined effect of the divergence of the fluxes that is the contribution of the turbulent transport, and the radioactive decay contribution (2). In order to understand which process is responsible for the collapse of the  $^{222}\text{Rn}$  and its short-lived daughters concentration in unsteady atmospheric boundary layers, we focus in the following on the vertical profiles of the radioactive decay contributions (Fig. 10) and fluxes (Fig. 11).

Under unsteady conditions, we found similar vertical profiles of the radioactive decay contribution to  $S_0$  progeny

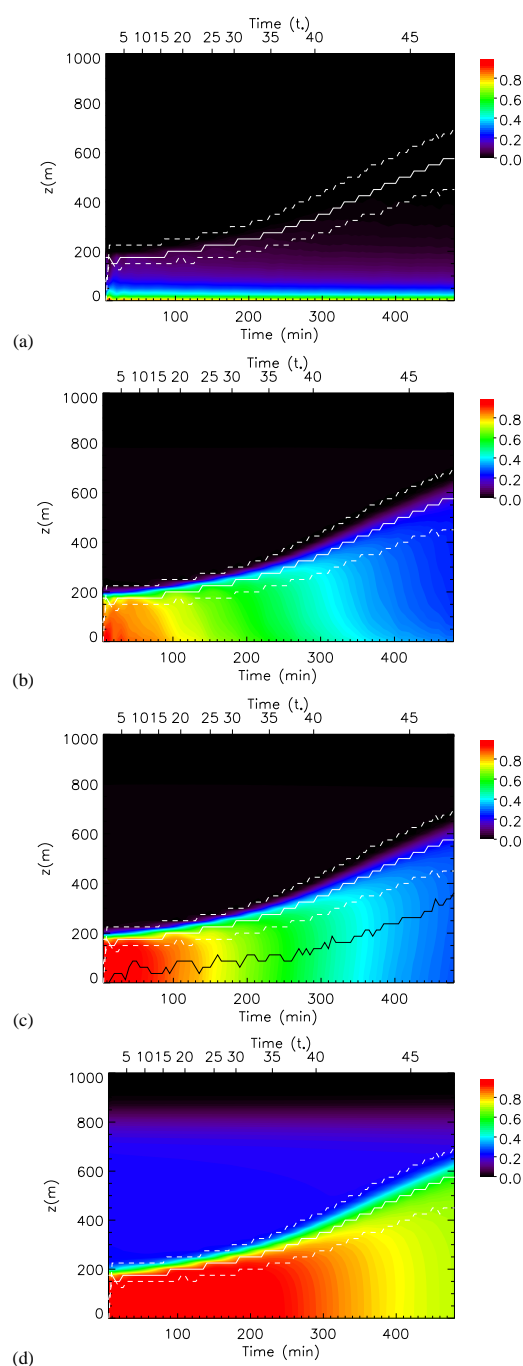


**Fig. 10.** Vertical profiles of the radioactive decay contributions to  $^{222}\text{Rn}$  progeny concentrations. Subfigures (a), (b), (c) and (d) are showing  $R_{S_1}$ ,  $R_{S_2}$ ,  $R_{S_3}$  and  $R_{S_4}$ , respectively. The top of the CBL is overlotted with a white solid line and the entrainment layer is located between the dashed white lines. As in Fig. 9, the steppy aspect of these latter quantities is due to the time averaging procedure. The location of the  $R_{S_3}$  maximum is also shown with a solid black line. The contributions have been made dimensionless using their maximum values. The profiles are plotted against time in minutes (lower x-axis) and in  $t_*$  (upper x-axis) where  $t_* = z_i/w_*$ .

concentrations as we found previously for the fully developed CBL. The radioactive decay term acts as a sink for  $S_0$  and as a source for its progeny. Moreover, the same vertical variations can be reported. All contributions show a maximum close to the surface except  $R_{S_3}$  and  $R_{S_4}$ . While the radioactive decay contribution to  $S_3$  concentration is maximum at the mid-CBL,  $R_{S_4}$  shows a well-mixed profile. Also a fast reduction of the decay contribution to  $S_2$  is found while moving upward.

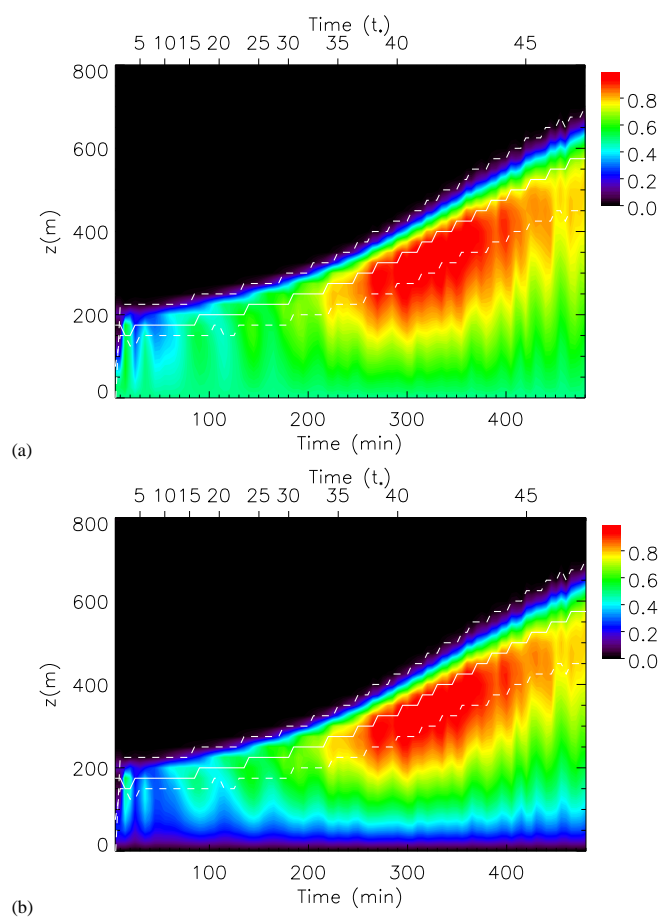
However, the variation with height of the radioactive decay contributions is enhanced while the boundary layer is deepening. As suggested by their turbulent Damköhler numbers shown in Table 2,  $S_1$ ,  $S_2$  and  $S_3$  are affected by the turbulent structures. Moreover since the  $Da_t$  are proportional to  $\tau_t$ , the  $Da_t$  increase together with the turbulent timescale. When the turnover time of the CBL is increasing, it takes more time for turbulence to transport and mix the compounds all over the boundary layer. As a result, the turbulent mixing of radon's daughters is less efficient and the vertical variation of the radioactive contribution is increasing with time.

Figure 11 shows the time evolution of the vertical fluxes for  $S_0$ , and  $S_1$ . The fluxes of the other daughters are not shown since they have similar shape as the ones of  $S_1$ . Actually for  $S_2$  and its daughters, we found the same behavior reported for the steady-state CBL: linear shapes (as suggested by the flux Damköhler numbers given in Table 3) with their maximum located close to the top of the boundary layer. Also suggested by the flux Damköhler numbers, only  $S_1$  fluxes show deviation from the inert shape and these deviations are decreasing with time as do the flux Damköhler numbers (from  $Da_{\overline{wS_1}}=0.62$  at the beginning of the simulation to  $Da_{\overline{wS_1}}=0.38$  at the end).

The most remarkable difference with the steady-state case is the behavior of  $S_0$ . In the steady-state CBL,  $S_0$  flux is a bottom-up flux with a maximum value at the surface (Fig. 5) whereas under unsteady conditions, the maximum  $S_0$  flux is moving toward the boundary layer top (Fig. 11a). Actually, the flux shows maximum values when the boundary layer growth rate is maximum. While the boundary layer is deepening, low  $^{222}\text{Rn}$  concentration air masses are entrained from the reservoir layer. Turbulence transport is balancing the gradient of concentration induced by the entrainment of cleaner air by transporting  $^{222}\text{Rn}$  towards the upper boundary layer. This upward flux is more vigorous when the ventilation process is enhanced by the increase of the boundary layer growth rate. Thus, the driving process responsible for the collapse of  $S_0$  concentration is much more likely the ventilation due to the entrainment of low-concentration air masses from the reservoir layer.

### 5.3 Role of entrainment on $^{222}\text{Rn}$ mixed-layer concentration

We have seen previously that entrainment plays a crucial role on the behavior of  $^{222}\text{Rn}$  and its progeny morning concen-



**Fig. 11.** Vertical profiles (a)  $^{222}\text{Rn}$  ( $S_0$ ) and (b)  $^{218}\text{Po}$  ( $S_1$ ) instantaneous fluxes. The fluxes are made dimensionless using their maximum values. The top of the CBL is overplotted with a white solid line and the entrainment layer is located between the dashed white lines. As in Figs. 9 and 10, the steppy aspect of these latter quantities is due to the time averaging procedure. The fluxes have been made dimensionless using their maximum values. The profiles are plotted against time in minutes (lower x-axis) and in  $t_*$  (upper x-axis) where  $t_* = z_i/w_*$ .

trations. The entrainment fluxes  $(\overline{wS_i})_e$  account for the exchange of compounds between the boundary layer and the free troposphere (or here the reservoir layer) and thus influence the vertical distribution of  $^{222}\text{Rn}$  and its daughters in the lower part of the troposphere. In the following, we focus on the entrainment flux to the surface flux ratio of  $^{222}\text{Rn}$ , i.e.  $\beta_0 = \frac{(\overline{wS_0})_e}{(\overline{wS_0})_s}$  where  $(\overline{wS_0})_e$  and  $(\overline{wS_0})_s$  are the entrainment and surface flux of  $S_0$  respectively, to outline the importance of the entrainment process. Figure 12 shows the time evolution of  $\beta$  (the ratio of entrainment to the surface flux of potential temperature),  $\beta_0$  and the mixed-layer concentration  $\langle S_0 \rangle$  calculated from the results obtained for the simulation of the convective boundary layer under unsteady conditions.

The calculation of  $\beta$  gives an almost constant value of  $\beta=0.2$  throughout the whole period of simulation. The  $\beta$

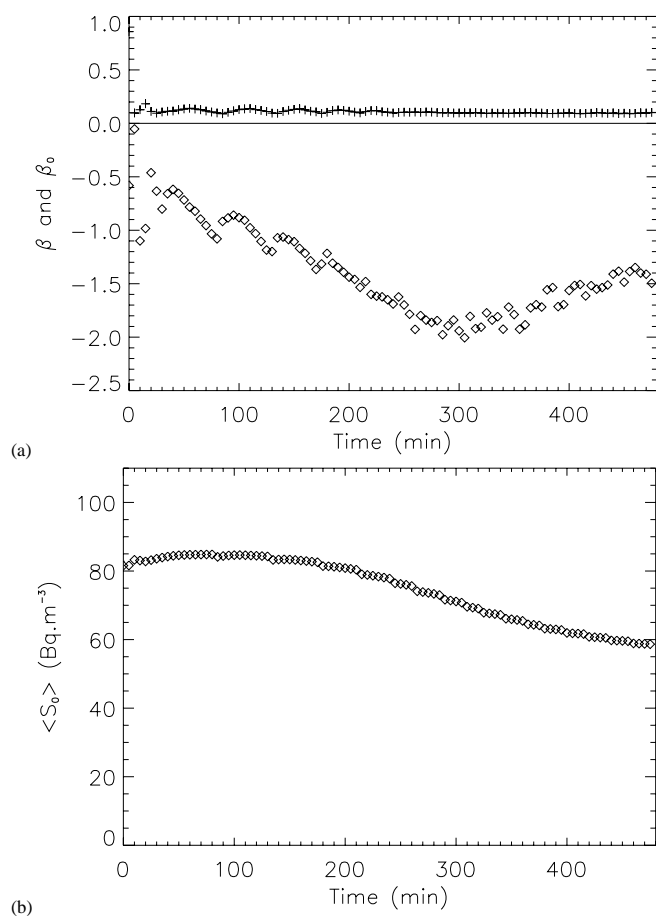


**Fig. 12.** Time evolution of (a) the ratios of the entrainment flux to the surface flux for potential temperature (crosses) and  $^{222}\text{Rn}$  (diamonds), and (b)  $^{222}\text{Rn}$  mixed-layer concentration  $\langle S_0 \rangle$ .

ratio is similar to other results obtained for CBLs simulated by a large-eddy simulation, moreover these studies show values ranging from 0.2 to 0.25 for buoyancy driven atmospheric boundary layers (van Zanten et al., 1999). The  $\beta$  values indicate that the turbulent eddies entrain warmer air from the free troposphere into the ABL. Since the reservoir layer concentrations are lower than the mixed layer ones, the entrained air is also cleaner (with lower concentrations of  $^{222}\text{Rn}$  and its progeny).

The  $\beta$  ratios for  $^{222}\text{Rn}$  are ranging from  $\beta_0 = -0.5$  to  $\beta_0 = -2$  and exhibits a maximum in absolute value at the time of the maximum growth of the boundary layer (at around  $t = 300$  min). The sign of the  $\beta_0$  indicates that, since  $^{222}\text{Rn}$  is emitted at the surface, the surface and the entrainment fluxes are both upward fluxes and so reveals the importance of the ventilation process at the top of the CBL. As can be clearly seen in Fig. 12b, the  $^{222}\text{Rn}$  mixed-layer concentration  $\langle S_0 \rangle$  exhibits two distinct periods. The first one (until 120 min) is characterized by the dominance of the emission from the surface (with  $|\beta_0| \leq 1$ ) and by the growth of the mixed layer

concentration. During the second period (after 2 h of simulation), the concentration is decreasing despite of the constant emission of  $^{222}\text{Rn}$  at the surface and the  $\beta_0$  show absolute values greater than 1. This correlation between the mixed layer concentration and  $\beta_0$  indicates that the main process responsible for the decrease of  $\langle S_0 \rangle$  is the mixing with low  $^{222}\text{Rn}$  concentration air originating from the reservoir layer. In other words, the ventilation induced by the deepening of the boundary layer enhances the entrainment flux leading to a decrease of the mixed layer concentration.

## 6 Summary and conclusions

The capacity of large-eddy simulation to perform accurate simulations of turbulent atmospheric boundary layers has been used to provide a complete and comprehensive analysis of the effect of turbulent transport on the distribution of  $^{222}\text{Rn}$  and its progeny. Studying how turbulent mixing controls the concentration and the distribution of decaying species with a wide range of half-lives allowed us to address the full range of atmospheric turbulent reacting flow, from slow to fast chemical regimes. Two representative cases are investigated: a steady state free convective atmospheric boundary layer and a CBL growing within a pre-existing reservoir layer.

Under steady state conditions, this analysis revealed that the concentrations are correlated with the half-life of the radioactive compounds and that the short-lived daughters' vertical distribution can be affected by the turbulent structure of the atmospheric boundary layer. Since the radioactive decay considered covers wide range of frequencies, even small vertical gradient of the concentrations can have important impact on the radioactive transformations due to the inefficient mixing of turbulence. In particular, the radioactive decay contribution to  $^{214}\text{Bi}$  exhibits a maximum 5% higher than the contribution calculated at the surface in the upper boundary layer. We showed that this profile was the result of the inability of turbulence to mix efficiently both  $^{218}\text{Po}$  and  $^{214}\text{Pb}$  in the CBL.

In addition, the fluxes of  $^{222}\text{Rn}$  and  $^{210}\text{Pb}$  have a linear profile whereas the ones of the other daughters show deviations from the linear shape. The deviations are due to the radioactive decaying process that acts as a source term in the flux budget. Using the appropriate Damköhler number, i.e. flux Damköhler number, assessed the relevance of radioactive decay contribution to the flux. This also allows classification of the daughters with respect to the effect of turbulent mixing on their vertical transport, e.g.  $^{214}\text{Pb}$  and  $^{214}\text{Bi}$  have similar decay frequencies but only  $^{214}\text{Pb}$  is significantly affected by turbulence. This analysis was confirmed by the explicit calculation of the different contributions to the flux budget equation. We also found that the gradient contribution to the flux is the most affected term meaning that the radioactive decay process is primary responsible for the relative decrease

of the concentration gradient. The exact decomposition also reveals that while  $^{222}\text{Rn}$  shows the typical bottom-up scalar flux behavior, the last daughter  $^{210}\text{Pb}$  exhibits the one of a top-down scalar.

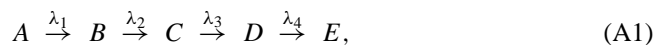
Under unsteady conditions,  $^{222}\text{Rn}$  and its short-lived daughter's concentrations decrease while the boundary layer deepens. This deepening leads to the increase of the turnover time of the CBL. Therefore it takes more time for turbulence to transport and mix the compounds all over the boundary layer. The fluxes are also affected by the deepening of the CBL. In particular, while  $^{222}\text{Rn}$  flux shows a maximum at the surface in the fully developed CBL, it is moving upwards under unsteady conditions and reaches a maximum for the fastest boundary layer growth. The analysis of the entrainment flux to the surface flux ratio correlated to the mixed-layer concentration of  $^{222}\text{Rn}$  showed that the growth of the boundary layer is inducing ventilation at the top of the CBL. The entrainment of cleaner air from the reservoir layer results in the decrease of the mixed layer concentrations.

From this comprehensive study, we can conclude that the turbulent properties of the atmospheric convective boundary layers are of importance to study the dispersion and the transport of the  $^{222}\text{Rn}$  family. The short-lived daughters are affected by the control exerts by turbulence on both their radioactive decay and their turbulent transport. Therefore accurate modeling requires accounting for the turbulent properties of the ABL. Finally, the turbulent and flux Damköhler numbers have shown to be useful dimensionless numbers to classify the effects of turbulent mixing on the concentration and the vertical transport of reacting scalars.

## Appendix A

### Analytical solution for $^{222}\text{Rn}$ and its progeny concentrations

For the chain of reactions



the chemical system that has to be solved is

$$\frac{dA}{dt} = -\lambda_1 A, \quad (\text{A2})$$

$$\frac{dB}{dt} = \lambda_1 A - \lambda_2 B, \quad (\text{A3})$$

$$\frac{dC}{dt} = \lambda_2 B - \lambda_3 C, \quad (\text{A4})$$

$$\frac{dD}{dt} = \lambda_3 C - \lambda_4 D, \quad (\text{A5})$$

$$\frac{dE}{dt} = \lambda_4 D. \quad (\text{A6})$$

For such a system with  $a_0$ ,  $b_0$ ,  $c_0$ ,  $d_0$  and  $e_0$  as initial concentrations of  $A$ ,  $B$ ,  $C$ ,  $D$  and  $E$  respectively, the analytical solutions read

$$A = a_0 e^{-\lambda_1 t}, \quad (\text{A7})$$

$$B = b_0 e^{-\lambda_2 t} + \frac{a_0 \lambda_1}{(\lambda_2 - \lambda_1)} (e^{-\lambda_1 t} - e^{-\lambda_2 t}), \quad (\text{A8})$$

$$C = c_0 e^{-\lambda_3 t} + \frac{a_0 \lambda_1 \lambda_2}{(\lambda_3 - \lambda_1)(\lambda_2 - \lambda_1)} (e^{-\lambda_1 t} - e^{-\lambda_3 t}) + \frac{\lambda_2}{(\lambda_3 - \lambda_2)} \left( b_0 - \frac{a_0 \lambda_1}{(\lambda_2 - \lambda_1)} \right) (e^{-\lambda_2 t} - e^{-\lambda_3 t}), \quad (\text{A9})$$

$$D = d_0 e^{-\lambda_4 t} + \frac{a_0 \lambda_1 \lambda_2 \lambda_3}{(\lambda_4 - \lambda_1)(\lambda_3 - \lambda_1)(\lambda_2 - \lambda_1)} (e^{-\lambda_1 t} - e^{-\lambda_4 t}) + \frac{\lambda_2 \lambda_3}{(\lambda_4 - \lambda_2)(\lambda_3 - \lambda_2)} \left( b_0 - \frac{a_0 \lambda_1}{(\lambda_2 - \lambda_1)} \right) (e^{-\lambda_2 t} - e^{-\lambda_4 t}) + \left[ c_0 - \frac{a_0 \lambda_1 \lambda_2}{(\lambda_3 - \lambda_1)(\lambda_2 - \lambda_1)} - \frac{\lambda_2}{(\lambda_3 - \lambda_2)} \left( b_0 - \frac{a_0 \lambda_1}{(\lambda_2 - \lambda_1)} \right) \right] \times \frac{\lambda_3}{(\lambda_4 - \lambda_3)} (e^{-\lambda_3 t} - e^{-\lambda_4 t}), \quad (\text{A10})$$

$$E = e_0 + (a_0 - A) + (b_0 - B) + (c_0 - C) + (d_0 - D). \quad (\text{A11})$$

These analytical solutions have been used to initialize the vertical profiles of  $^{222}\text{Rn}$  and its progeny in the reservoir layer for the unsteady condition simulation. In the nocturnal boundary layer (NBL),  $^{222}\text{Rn}$  is continuously emitted at the surface and is assumed to be instantaneously mixed within the NBL of depth  $z_i$ . In the previous system, this situation corresponds to the injection of fresh material of  $A$ , thus  $A$  time evolution concentration now read

$$\frac{dA}{dt} = -\frac{(F_{z_i} - F_s)}{z_i} - \lambda_1 A, \quad (\text{A12})$$

where the vertical flux divergence is approximated by the ratio of the net flux, i.e. the difference between the surface flux  $F_s$  and the detrainment flux at the top of the CBL  $F_{z_i}$ , to the boundary layer depth  $z_i$ . Assuming that  $F_{z_i} < F_s$ , the analytical solutions of the system become

$$A = \frac{F_s}{\lambda_1 z_i} + \alpha e^{-\lambda_1 t}, \quad (\text{A13})$$

$$B = \frac{F_s}{\lambda_2 z_i} + \beta e^{-\lambda_2 t} + \frac{\alpha \lambda_1}{(\lambda_2 - \lambda_1)} (e^{-\lambda_1 t} - e^{-\lambda_2 t}), \quad (\text{A14})$$

$$C = \frac{F_s}{\lambda_3 z_i} + \chi e^{-\lambda_3 t} + \frac{\alpha \lambda_2 \lambda_1}{(\lambda_3 - \lambda_1)(\lambda_2 - \lambda_1)} (e^{-\lambda_1 t} - e^{-\lambda_3 t}) + \frac{\lambda_2}{(\lambda_3 - \lambda_2)} \left( \beta - \frac{\alpha \lambda_1}{(\lambda_2 - \lambda_1)} \right) (e^{-\lambda_2 t} - e^{-\lambda_3 t}), \quad (\text{A15})$$

$$\begin{aligned}
D = & \frac{F_s}{\lambda_4 z_i} + \delta e^{-\lambda_4 t} + \frac{\alpha \lambda_3 \lambda_2 \lambda_1}{(\lambda_4 - \lambda_1)(\lambda_3 - \lambda_1)(\lambda_2 - \lambda_1)} (e^{-\lambda_1 t} - e^{-\lambda_4 t}) \\
& + \frac{\lambda_3 \lambda_2}{(\lambda_4 - \lambda_2)(\lambda_3 - \lambda_2)} \left[ \beta - \frac{\alpha \lambda_1}{(\lambda_2 - \lambda_1)} \right] (e^{-\lambda_2 t} - e^{-\lambda_4 t}) \\
& + \left[ \chi - \frac{\alpha \lambda_2 \lambda_1}{(\lambda_3 - \lambda_1)(\lambda_2 - \lambda_1)} - \frac{\lambda_2}{(\lambda_3 - \lambda_2)} \left( \beta - \frac{\alpha \lambda_1}{(\lambda_2 - \lambda_1)} \right) \right] \\
& \times \frac{\lambda_3}{(\lambda_4 - \lambda_3)} (e^{-\lambda_3 t} - e^{-\lambda_4 t}), \tag{A16}
\end{aligned}$$

$$\begin{aligned}
E = & e_0 + \frac{F_s}{z_i} t + \frac{\alpha \lambda_4 \lambda_3 \lambda_2}{(\lambda_4 - \lambda_1)(\lambda_3 - \lambda_1)(\lambda_2 - \lambda_1)} (e^{-\lambda_1 t} - 1) \\
& + \frac{\lambda_4 \lambda_3}{(\lambda_4 - \lambda_2)(\lambda_3 - \lambda_2)} \left( \beta - \frac{\alpha \lambda_1}{(\lambda_2 - \lambda_1)} \right) (e^{-\lambda_2 t} - 1) \\
& + \frac{\lambda_4}{(\lambda_4 - \lambda_3)} \left[ \chi - \frac{\alpha \lambda_2 \lambda_1}{(\lambda_3 - \lambda_1)(\lambda_2 - \lambda_1)} - \frac{\lambda_2}{(\lambda_3 - \lambda_2)} \left( \beta - \frac{\alpha \lambda_1}{(\lambda_2 - \lambda_1)} \right) \right] (e^{-\lambda_3 t} - 1) \\
& - \left[ \frac{\lambda_3 \lambda_2}{(\lambda_4 - \lambda_2)(\lambda_3 - \lambda_2)} \left( \beta - \frac{\alpha \lambda_1}{(\lambda_2 - \lambda_1)} \right) + \frac{\alpha \lambda_3 \lambda_2 \lambda_1}{(\lambda_4 - \lambda_1)(\lambda_3 - \lambda_1)(\lambda_2 - \lambda_1)} \right] \\
& + \frac{\lambda_3}{(\lambda_4 - \lambda_3)} \left[ \chi - \frac{\alpha \lambda_2 \lambda_1}{(\lambda_3 - \lambda_1)(\lambda_2 - \lambda_1)} - \frac{\lambda_2}{(\lambda_3 - \lambda_2)} \left( \beta - \frac{\alpha \lambda_1}{(\lambda_2 - \lambda_1)} \right) \right] + \delta \Big] \\
& \times (e^{-\lambda_4 t} - 1), \tag{A17}
\end{aligned}$$

where

$$\begin{aligned}
\alpha &= a_0 - \frac{F_s}{\lambda_1 z_i}, \\
\beta &= b_0 - \frac{F_s}{\lambda_2 z_i}, \\
\chi &= c_0 - \frac{F_s}{\lambda_3 z_i}, \\
\delta &= d_0 - \frac{F_s}{\lambda_4 z_i}. \tag{A18}
\end{aligned}$$

**Acknowledgements.** All computations were performed on the Linux cluster of the ECOMAR action of the Institute for Environment and Sustainability. The authors wish to thank A. Stips and P. Simons who kindly provided the access to this facility. The authors are thankful to both referees, J. Vilà-Guerau de Arellano and A. G. Williams, for their comments and remarks.

Edited by: M. G. Lawrence

## References

- Allen, D. J., Rood, R. B., Thompson, A. M., and Hudson R. D.: Three-dimensional radon-222 calculations using assimilated meteorological data and a convective mixing algorithm, *J. Geophys. Res.*, 101, 6871–6881, 1996.
- Beck, H. L. and Gogolak C. V.: Time dependent calculation of the vertical distribution of  $^{222}\text{Rn}$  and its decay products in the atmosphere, *J. Geophys. Res.*, 84, 3139–3148, 1979.
- Butterweck, G., Reineking, A., Kesten, J., and Porstendörfer J.: The use of the natural radioactive noble gases radon and thoron as tracers for the study of the turbulent exchange in the atmospheric boundary layer case study in and above a wheat field, *Atmos. Environ.* 28, 1963–1969, 1994.
- Clarke, R. H., Dyer, A. J., Brook, R. R., Reid, D. G., and Troup A. J.: The Wangara experiment: boundary layer data, Paper No. 19, Div. Meteorol. Phys., CSIRO, Australia, 1971.

- Cuijpers, J. W. M. and Duynkerke P. G.: Large eddy simulations of trade wind with cumulus clouds, *J. Atmos. Sci.* 50, 3894–3908, 1993.
- Cuijpers, J. W. M. and Holtslag A. A. M.: Impact of skewness and nonlocal effects on scalar and buoyancy fluxes in convective boundary layers, *J. Atmos. Sci.*, 55, 151–162, 1998.
- Damköhler, G.: Influence of turbulence on the velocity flames in gas mixtures, *Z. Elektrochem.*, 46, 601–626, 1940.
- Deardorff, J. W.: Three-dimensional numerical study of turbulence in an entraining mixed layer, *Bound.-Layer Meteorol.*, 7, 199–226, 1974.
- Deardorff, J. W.: Prediction of convective mixed-layer entrainment for realistic capping inversion structure, *J. Atmos. Sci.*, 36, 424–436, 1979.
- Dentener, F., Feichter, J., and Jeuken A.: Simulation of the transport of Rn-222 using on-line and off-line global models at different horizontal resolutions: a detailed comparison with measurements, *Tellus 51B*, 573–602, 1999.
- Druilhet, A. and Fontan J.: Détermination des coefficients de diffusion verticale entre 0 et 100 m à l'aide du radon et du ThB, *Bound.-Layer Meteorol.*, 3, 468–498, 1973a.
- Druilhet, A. and Fontan J.: Utilisation du thoron pour la détermination du coefficient vertical de diffusion turbulente près de sol, *Tellus 25*, 199–212, 1973b.
- Fontan, J., Guedalia, D., Druilhet, A., and Lopez A.: Une méthode de mesure de la stabilité verticale de l'atmosphère près du sol, *Bound.-Layer Meteorol.*, 17, 3–14, 1979.
- Fujinami, N. and Esaka S.: Variations in Radon 222 daughter concentrations in surface air with atmospheric stability, *J. Geophys. Res.*, 92, 1041–1043, 1987.
- Fujinami, N. and Esaka S.: A simple model for estimating the mixing depth from the diurnal variation of atmospheric  $^{222}\text{Rn}$  concentration, *Rad. Prot. Dos.*, 24, 88–91, 1988.
- Galmarini, S.: One year of  $^{222}\text{Rn}$  concentration in the atmospheric surface layer, *Atmos. Chem. Phys.* 6, 2865–2887, 2006.
- Gao, W. and Wesely M. L.: Numerical modelling of the turbulent fluxes of chemically reactive trace gases in the atmospheric boundary layer, *J. Appl. Meteorol.*, 33, 835–847, 1994.
- Guedalia, D., Allet, C., Fontan, J., Druilhet, A., and Assaf, G.: Lead-212, Rn, and vertical mixing in the lower atmosphere (100–2000 m), *Tellus*, 25, 381–385, 1973.
- Guedalia, D., Allet, C., and Fontan J.: Vertical exchange measurements in the lower troposphere using ThB ( $^{212}\text{Pb}$ ) and radon ( $^{222}\text{Rn}$ ), *J. Appl. Meteorol.*, 13, 27–39, 1974.
- Guedalia, D., NTsila, A., Druilhet, A., and Fontan J.: Monitoring of the atmospheric stability above an urban and suburban site using rodar and radon measurements, *J. Appl. Meteorol.*, 19, 839–848, 1980.
- Gaudry, A., Polian, G., Ardouin, B., and Lambert G.: Radon-calibrated emissions of CO<sub>2</sub> from South Africa, *Tellus*, 42B, 9–19, 1990.
- Genthon, C. and Armengaud A.: Radon-222 as a comparative tracer of transport and mixing in 2 general-circulation models of the atmosphere, *J. Geophys. Res.*, 100, 2849–2866, 1995.
- Ikebe, Y.: Variation of radon and thoron concentrations in relation to the wind speed, *J. Meteorol. Soc. Jpn.*, 48, 461–467, 1970.
- Ikebe, Y. and Shimo M.: Estimation of the vertical turbulent diffusivity from thoron profiles, *Tellus*, 24, 29–37, 1972.
- Jacob, D. J. and Prather M. J.: Radon-222 as a test of convective

- transport in a general circulation model, *Tellus*, 42B, 118-134, 1990.
- Jacob, D. J., Prather, M. J., Rasch, P. J., Shia, R. L., Balkanski, Y. J., Beagley, S. R., Bergmann, D. J., Blackshear, W. T., Brown, M., Chiba, M., Chipperfield, M. P., deGrandpre, J., Dignon, J. E., Feichter, J., Genthon, C., Grose, W. L., Kasibhatla, P. S., Kohler, I., Kritz, M. A., Law, K., Penner, J. E., Ramonet, M., Reeves, C. E., Rotman, D. A., Stockwell, D. Z., VanVelthoven, P. F. J., Verver, G., Wild, O., Yang, H., and Zimmermann P.: Evaluation and intercomparison of global atmospheric transport models using Rn-222 and other short-lived tracers, *J. Geophys. Res.*, 102, 5953–5970, 1997.
- Jacobi, W. and Andre K.: The vertical distribution of  $^{222}\text{Rn}$ ,  $^{220}\text{Rn}$  and their decay products in the atmosphere, *J. Geophys. Res.*, 68, 3799–3814, 1963.
- Jonker, H. J. J., Vilà -Guerau de Arellano, J., and Duijkerke P. G.: Characteristic length scales of reactive species in a convective boundary layer, *J. Atmos. Sci.*, 61, 41–56, 2004.
- Kataoka, T., Yunoki, E., Shimizu, M., Mori, T., Tsukamoto, O., Ohhashi, Y., Sahashi, K., Maitani, T., Miyashita, K., Fujikawa, Y., and Kudo A.: Diurnal variation in radon concentration and mixing-layer depth, *Bound.-Layer Meteorol.*, 89, 225-250, 1998.
- Kataoka, T., Yunoki, E., Shimizu, M., Mori, T., Tsukamoto, O., Ohhashi, Y., Sahashi, K., Maitani, T., Miyashita, K., Iwata, T., Fujikawa, Y., Kudo, A., and Shaw R. H.: A study of the atmospheric boundary layer using radon and air pollutants as tracers, *Bound.-Layer Meteorol.*, 101, 131-155, 2001.
- Krol, M. C., Molemaker, M. J., and Vilà-Guerau de Arellano J.: Effects of turbulence and heterogeneous emissions on photochemically active species in the convective boundary layer, *J. Geophys. Res.*, 105, 6871–6884, 2000.
- Larson, R. E., Lamontagne, R. A., and Wittmann W. I.: Radon-222, CO, CH<sub>4</sub> and continental dust over the greenland and norwegian seas, *Nature*, 240, 345-347, 1972.
- Li, Y. H. and Chang J. S.: A three-dimensional global episodic tracer transport model. I. Evaluation of its processes by radon 222 simulations, *J. Geophys. Res.*, 101, 25 931–25 947, 1996.
- Lopez, A., Guedalia, D., Servant, J., and Fontan J.: Advantages of the use of radioactive tracers  $^{222}\text{Rn}$  and  $^{212}\text{Pb}$  for the study of aiken nuclei within the lower troposphere, *J. Geophys. Res.*, 79, 1243-1252, 1974.
- Mahowald, N. M., Rasch, P. J., Eaton, B. E., Whittlestone, S., and Prinn R. G.: Transport of ( $^{222}\text{Rn}$ ) radon to the remote troposphere using the model of atmospheric transport and chemistry and assimilated winds from ECMWF and the National Center for Environmental Prediction NCAR, *J. Geophys. Res.*, 102, 28 139-28 151, 1997.
- Moeng, C. H. and Wyngaard J. C.: Statistics of conservative scalars in the convective boundary layer, *J. Atmos. Sci.*, 41, 3161–3169, 1984.
- Molemaker, M. J. and Vilà-Guerau de Arellano J.: Turbulent control of chemical reactions in the convective boundary layer, *J. Atmos. Sci.*, 55, 568–579, 1998.
- Moses, H., Lucus Jr., H. F., and Zerbe G. A.: The Effect of Meteorological Variables upon Radon concentration three feet above the ground, *J. Air Pollut. Control. Assoc.*, 13, 12-19, 1963.
- Patton, E. G., Davis, K. J., Barth, M. C., and Sullivan P. P. : Decaying scalars emitted by a forest canopy: a numerical study, *Bound.-Layer Meteorol.*, 100, 91–129, 2001.
- Pearson, J. E. and Moses H.: Atmospheric Radon-222 concentration variation with height and time, *J. Appl. Meteorol.* 5, 175-181, 1966.
- Petersen, A. C. and Holtslag A. A. M.: A first-order closure for covariances and fluxes of reactive species in the convective boundary layer, *J. Appl. Meteorol.*, 38, 1758–1776, 1999.
- Petersen, A. C., Beets, C., van Dop, H., and Duijkerke P. G.: Mass-flux schemes for transport of non-reactive and reactive scalars in the convective boundary layer, *J. Atmos. Sci.*, 56, 37–56, 1999.
- Petersen, A. C.: The impact of chemistry on flux estimates in the convective boundary layer, *J. Atmos. Sci.*, 57, 3398–3405, 2000.
- Polian, G., Lambert, G., Ardouin, B., and Jegou A.: Long-range transport of continental radon in subantarctic and antarctic areas, *Tellus*, 38B, 178-189, 1986.
- Porstendörfer, J.: Properties and behaviour of radon and thoron and their decay products in the air, *J. Atmos. Sci.*, 25, 219–263, 1994.
- Ramonet, M., Le Roulley, J. C., Bousquet, P., and Monfray P.: Radon-222 measurements during the Tropoz II campaign and comparison with a global atmospheric transport model, *J. Atmos. Chem.*, 23, 107-136, 1996.
- Robé, M. C., Rannou, A., and Le Bronec J. Radon measurement in the environment in France, *Rad. Prot. Dos.*, 45, 455-457, 1992.
- Schumann, U.: Large-eddy simulation of turbulent diffusion with chemical reactions in the convective boundary layer, *Atmos. Environ.*, 23, 1713–1729, 1989.
- Sykes, R. I., Parker, S. F., Henn, D. S., and Lewellen W. S.: Turbulent mixing with chemical reactions in the planetary boundary layer, *J. Appl. Meteorol.*, 33, 825–834, 1994.
- Sesana, L., Barbieri, L., Facchini, U., and Marazzan G.M.:  $^{222}\text{Rn}$  as a tracer of atmospheric motions: a study in Milan, *Rad. Prot. Dos.*, 78, 65–71, 1998.
- Sesana, L., Ottobri, B., Polla, G., and Facchini U.:  $^{222}\text{Rn}$  as indicator of atmospheric turbulence: measurements at Lake Maggiore and on the pre-Alps, *J. Env. Rad.*, 86, 271–288, 2006.
- Siebesma, A. P. and Cuijpers J. W. M.: Evaluation of parametric assumptions for shallow cumulus convection, *J. Atmos. Sci.*, 52, 650–666, 1995.
- Stockwell, D. Z., Kritz, M. A., Chipperfield, M. P., and Pyle J. A.: Validation of an off-line three dimensional chemical transport model using observed radon profiles – 2. Model results, *J. Geophys. Res.*, 103, 8433-8445, 1998.
- van Zanten, M., Duijkerke, P. G., and Cuijpers J. W. M.: Entrainment parameterizations in convective boundary layers, *J. Atmos. Sci.*, 56, 813-828, 1999.
- Verver, G. H. L., van Dop, H., and Holtslag A. A. M.: Turbulent mixing of reactive gases in the convective boundary layer, *Bound.-Layer Meteorol.*, 85, 197–222, 1997.
- Vilà-Guerau de Arellano, J., and Cuijpers J. W. M.: The chemistry of a dry cloud: the effects of radiation and turbulence, *J. Atmos. Sci.* 57, 1573–1584, 2000.
- Vilà-Guerau de Arellano J.: Bridging the gap between atmospheric physics and chemistry in studies of small-scale turbulence, *Bull. Amer. Meteor. Soc.*, 84, 51–56, 2003.
- Vinod Kumar, A., Sitaraman, V., Oza, R. B., and Krishamoorthy T. M.: Application of a numerical model for the planetary boundary layer to the vertical distribution of radon and its daughter products, *Atmos. Environ.*, 33, 4717–4726, 1999.
- Vinuesa, J.-F. and Vilà -Guerau de Arellano J.: Fluxes and (co-)variances of reacting scalars in the convective boundary layer,

- Tellus, 55B, 935-949, 2003.
- Vinuesa, J.-F. and Vilà -Guerau de Arellano J.: Introducing effective reaction rates to account for the inefficient mixing of the convective boundary layer, Atmos. Environ., 39, 445–461, 2005.
- Wilkening M. H.: Radon 222 concentrations in the convective patterns of a mountain environment, J. Geophys. Res., 75, 1733–1740, 1970.
- Wyngaard, J. C. and Brost R. A.: Top-down and bottom-up diffusion of a scalar in the convective boundary layer, J. Atmos. Sci., 41, 102–112, 1984.
- Wyngaard J. C.: Structure of the planetary boundary layer and implications for its modeling, J. Clim. App. Meteorol., 24, 1131–1142, 1985.
- Zahorowski, W., Chambers, S. D., and Henderson-Sellers, A.: Ground based radon-222 observations and their application to atmospheric studies, J. Env. Rad., 76, 3-33, 2004.